



An Active Plume Eruption on Europa During Galileo Flyby E26 as Indicated by Energetic Proton Depletions

H. L. F. Huybrighs, E. Roussos, A. Blöcker, N. Krupp, Y. Futaana, S. Barabash, Lina Hadid, M. K. G. Holmberg, O. Lomax, O. Witasse

► To cite this version:

H. L. F. Huybrighs, E. Roussos, A. Blöcker, N. Krupp, Y. Futaana, et al.. An Active Plume Eruption on Europa During Galileo Flyby E26 as Indicated by Energetic Proton Depletions. *Geophysical Research Letters*, 2020, 47 (10), pp.e2020GL087806. 10.1029/2020GL087806 . hal-02714020

HAL Id: hal-02714020

<https://hal.science/hal-02714020v1>

Submitted on 16 Sep 2022

HAL is a multi-disciplinary open access archive for the deposit and dissemination of scientific research documents, whether they are published or not. The documents may come from teaching and research institutions in France or abroad, or from public or private research centers.

L'archive ouverte pluridisciplinaire **HAL**, est destinée au dépôt et à la diffusion de documents scientifiques de niveau recherche, publiés ou non, émanant des établissements d'enseignement et de recherche français ou étrangers, des laboratoires publics ou privés.



Geophysical Research Letters

RESEARCH LETTER

10.1029/2020GL087806

Key Points:

- Energetic proton flux depletions during Galileo flyby E26 are driven by inhomogeneous fields, atmospheric charge exchange, and a plume
- Plumes can deplete protons through charge exchange and field perturbations
- Plumes are a source of energetic neutral atoms

Supporting Information:

- Supporting Information S1
- Figure S1
- Figure S2
- Figure S3
- Figure S4
- Figure S5
- Figure S6

Correspondence to:

H. L. F. Huybrighs,
hans.huybrighs@esa.int

Citation:

Huybrighs, H. L. F., Roussos, E., Blöcker, A., Krupp, N., Futaana, Y., Barabash, S., et al. (2020). An active plume eruption on Europa during Galileo flyby E26 as indicated by energetic proton depletions. *Geophysical Research Letters*, 47, e2020GL087806. <https://doi.org/10.1029/2020GL087806>

Received 4 MAR 2020

Accepted 17 APR 2020

Accepted article online 29 APR 2020

An Active Plume Eruption on Europa During Galileo Flyby E26 as Indicated by Energetic Proton Depletions

H. L. F. Huybrighs¹ , E. Roussos² , A. Blöcker³ , N. Krupp² , Y. Futaana⁴ , S. Barabash⁴, L. Z. Hadid⁵ , M. K. G. Holmberg¹ , O. Lomax¹, and O. Witasse¹

¹ESA/ESTEC, Noordwijk, Netherlands, ²Max Planck Institute for Solar System Research, Göttingen, Germany, ³KTH, Royal Institute of Technology, Stockholm, Sweden, ⁴IRF, Swedish Institute of Space Physics, Kiruna, Sweden, ⁵LPP, CNRS, École polytechnique, Sorbonne Université, Observatoire de Paris, Université Paris-Saclay, PSL Research University, Paris, France

Abstract Strong depletions of energetic protons (115–244 keV) were observed during Galileo flyby E26 of Europa. We simulate the flux of energetic protons using a Monte Carlo particle backtracing code and show that energetic proton depletions during E26 are reproduced by taking into account the perturbations of the electromagnetic fields calculated by magnetohydrodynamic (MHD) simulations and charge exchange with a global atmosphere and plume. A depletion feature occurring shortly after closest approach is driven by plume associated charge exchange, or a combination with plume associated field perturbations. We therefore conclude, with a new method and independent data set, that Galileo could have encountered a plume during E26.

Plain Language Summary We investigate why (normally abundant) fast protons were disappearing during Europa flyby E26 by Galileo. We do this by simulating the proton motion. In some cases we detect few protons because Europa is blocking the field of view. What is new here is that part of the decrease can be explained by charge exchange, a process whereby the protons are removed after they lose their electrical charge in Europa's thin atmosphere. Furthermore, we see that there is a special decrease, which can be explained by an erupting plume of water vapor, thereby providing additional evidence for an active plume during Galileo flyby E26.

1. Introduction

Europa, the fourth largest moon of Jupiter (radius = 1,562 km), is thought to harbor a potentially habitable water ocean under its surface. It resides in Jupiter's inner magnetosphere at a distance of 9.38 Jupiter radii. Here it is exposed to two populations of charged particles: relatively low-energy corotating plasma and highly energetic charged particles (Kivelson et al., 2009). Europa, its atmosphere, and its plumes affect the local magnetospheric environment. In particular, depletions of the energetic ion flux were measured by the Energetic Particle detector (EPD) (Williams et al., 1992) during Galileo flybys of Europa. Paranicas et al. (2000) attributes depletions during flyby E12 to ions impacting the surface of Europa, and to drift motions resulting from gradients in the inhomogeneous magnetic field. Near-Europa perturbations in the electromagnetic field are caused by the interaction of the magnetospheric plasma with Europa's tenuous atmosphere and by the signal from a subsurface water ocean due to Jupiter's time-varying magnetic field in Europa's reference frame. A magnetic field gradient can restrict access of the ions in a certain region, creating a "forbidden region." Paranicas et al. (2007) previously reported that energetic ions (120–280 keV) were depleted around the closest approach of the E26 flyby and attribute these depletions to absorption by Europa's surface.

Depletions of protons (80–220 keV) by charge exchange with Europa's neutral torus were reported by Lagg et al. (2003) and Kollmann et al. (2016). However, these studies did not address depletions during close flybys of Europa. Water vapor plumes provide an additional source of neutrals. Their existence has been suggested by multiple studies (De La Fuente Marcos & Nissar, 2000; Jia et al., 2018; McGrath & Sparks, 2017; Paganini et al., 2019; Roth et al., 2014; Sparks et al., 2016, 2017, 2019). Additionally, plasma interaction with plumes also cause perturbations in the magnetic field, which could also affect ion trajectories

©2020. The Authors.

This is an open access article under the terms of the Creative Commons Attribution License, which permits use, distribution and reproduction in any medium, provided the original work is properly cited.

(Arnold et al., 2019; Blöcker et al., 2016; Jia et al., 2018). Furthermore, Blöcker et al. (2016) and Arnold et al. (2019) have argued previously, based on magnetic field measurements by Galileo, that a plume was encountered during E26. Breer et al. (2019) has shown that the access of energetic ions to the surface of Europa is affected by inhomogeneous fields resulting from the plasma interaction with Europa's atmosphere and plumes.

In this work we investigate the cause of the depletions during E26 by simulating the flux of energetic protons using a Monte Carlo particle backtracing method. Note that we refer to any kind of flux dropout as “depletion,” be it due to surface impact, charge exchange, or Galileo encountering a “forbidden region.” Particle tracing studies have been conducted at various moons, for example, at Jupiter's moons Europa (Breer et al., 2019; Cassidy et al., 2013), Ganymede (Carnielli et al., 2019), and Callisto (Liuzzo et al., 2019), at Titan (Regoli et al., 2016), at Earth's Moon using backtracing (Futaana et al., 2003), or at Mars and Phobos (Curry et al., 2014; Futaana et al., 2010). Ion depletions have been investigated using particle tracing, for example, at the Jovian moon Io and Ganymede (Poppe et al., 2018; Selesnick & Cohen, 2009) and Saturnian moons Dione, Rhea, and Titan (Kotova et al., 2015; Wulms et al., 2010). We investigate the following possible contributing factors to the depletions: impact on the surface, atmospheric charge exchange, inhomogeneous fields due to the plasma interaction with the atmosphere, and the effect of plumes (both charge exchange and field perturbations).

The EPD proton channel TP1 (115–244 keV) is particularly suitable for this study. Channel TP1 is part of the Composition Measurement System (CMS) of the EPD telescope. CMS uses a time of flight mass spectrometer to separate protons from other ions and a triple coincidence detection system to limit the effect of noise by penetrating radiation. Furthermore, the cross section for charge exchange between H^+ and O_2 at the energies covered by TP1 is the largest compared to the other (higher-) energy proton channels (see Figure S1 in the supporting information). Moreover, compared to other measured ion species (e.g., oxygen or sulfur), less-free parameters are involved, as the protons have a known charge state, while oxygen and sulfur could have higher charge states (Clark et al., 2016; Nénon & André, 2019). Additionally, there are large uncertainties in the charge exchange cross section for those species. Finally, the energies involved are high enough to result in a gyroradius comparable to the spacecraft altitude (see Figure S2) and allow for surface impact, and also small enough for gyration scales to be sensitive to inhomogeneous fields.

2. Method

We simulate the flux of energetic protons using a Monte Carlo particle backtracing code, developed from Huybrighs et al. (2017). Energetic ions can be treated as test particles that have no influence on the electromagnetic fields, as their energy density is small compared to that of the low energy plasma. In the simulation the spacecraft trajectory is divided in different time steps. At each time step the proton flux is simulated, taking into account the spin of the spacecraft and the motion of EPD CMS relative to the spacecraft. For each proton, it is determined if it impacts and/or charge exchanges. By performing this analysis for many particles, the depletion is determined as a fraction of the (normalized) undisturbed flux.

Using the Monte Carlo method, particles are launched at a random, but uniformly distributed, angle within the instrument opening cone (18°) and at a random energy within the energy range of the TP1 channel. The energy range of TP1 at the beginning of the mission was from 80 to 220 keV. Due to the growth of an insensitive layer in the silicon detector (“dead layer”) by the time of E26, the energy range is expected to be from 115 to 244 keV (Lee-Payne et al., 2020).

Trajectories of protons are determined by numerically integrating the Lorentz force using a leap frog integration scheme (Huybrighs et al., 2017). Ion trajectories are traced back in time from the detector. The backtracing method results in a reduction of computing resources compared to forward tracing, as only the trajectories of particles that could enter the detector are simulated. Parameter settings for the particle tracing are summarized in Table 1; additional details are in the supporting information.

To simulate the trajectories of energetic ions, a description of the electromagnetic field is required. We consider both a homogeneous field and an inhomogeneous field. The homogeneous \mathbf{B} field is based on the Galileo MAG data. The electric field \mathbf{E} is calculated from \mathbf{B} using the relation $\mathbf{E} = -\mathbf{v} \times \mathbf{B}$, in which \mathbf{v} is the velocity of the corotational plasma. The inhomogeneous field takes into account the perturbations in the electromagnetic field resulting from the interaction of Europa's atmosphere with the low-energy

Table 1
Parameter Values Used in the Simulations

Parameters	Value
particle tracing simulation	
Integration time step particle trajectory [s]	0.002
Maximum number of time steps per particle	50,000
Number of particles per looking direction	100
Number of energy bins	10
Spacecraft trajectory time step [s]	0.6
Parameters MHD simulation	Value
Plume location (θ, ϕ)	(140°, 60°)
Plume scale height (H_p) [km]	200
Plume opening angle (θ_p) [deg]	15
Plume surface density (N_{P0}) [cm^{-3}]	$2.5 \times 10^8, \mathbf{2.5 \times 10^9}, 2.5 \times 10^{10}$
Sublimated atmosphere scale height (h_{s1}) [km]	100
Sputtered atmosphere scale height (h_{s2}) [km]	500
Sublimated atmosphere surface density (n_{10}) [cm^{-3}]	$2 \times 10^7, \mathbf{2.5 \times 10^7}$
Sputtered atmosphere surface density (n_{20}) [cm^{-3}]	1×10^6
Magnetospheric plasma density [cm^{-3}]	21
Magnetospheric plasma velocity (v_x) [km/s]	104
Background magnetic field (B_x, B_y, B_z) [nT]	(−22, 205, −379)
Internal energy density [nPa]	0.44

Note. MHD parameters based on Blöcker et al. (2016) and references therein. Where multiple values are considered, bold values indicate the default values.

plasma, including the contribution of plumes. The inhomogeneous fields are obtained from simulations of a three-dimensional magnetohydrodynamic (MHD) model performed on a spherical grid. The values for \mathbf{B} and \mathbf{v} in the homogeneous case are the same as those used for the MHD simulation (see Table 1). The MHD model was applied in previous studies to investigate the influence of inhomogeneities in Europa's atmosphere (e.g., water vapor plumes) on Europa's plasma interaction with Jupiter's magnetosphere (Blöcker et al., 2016) and the effect of atmospheric asymmetries on Io's plasma interaction (Blöcker et al., 2018). The MHD model is a modified version of the ZEUS-MP MHD code (Hayes et al., 2006; Norman, 2000). The modifications of the code are described in detail in Blöcker et al. (2016). An overview of the parameter settings for the simulation is given in Table 1; additional details are in the supporting information. The MHD model takes into account collisions between ions and neutrals, plasma production and loss due to electron impact ionization, dissociative recombination, and electromagnetic induction in a subsurface water ocean.

The density of Europa's molecular oxygen atmosphere (N_n) is prescribed within the code with an analytic expression following equation (1) from Jia et al. (2018):

$$N_n = \begin{cases} (1 + 2 \cos \tilde{\phi}) \cdot \left[n_{10} \exp\left(\frac{R_E - r}{h_{s1}}\right) + n_{20} \exp\left(\frac{R_E - r}{h_{s2}}\right) \right], & \text{if } \tilde{\phi} \leq 90^\circ \\ n_{10} \exp\left(\frac{R_E - r}{h_{s1}}\right) + n_{20} \exp\left(\frac{R_E - r}{h_{s2}}\right), & \text{if } \tilde{\phi} > 90^\circ \end{cases}. \quad (1)$$

Jia et al. (2018) accounts by the azimuthal angle $\tilde{\phi}$ (measured from the negative x axis in EPhIO; see the supporting information) for higher neutral densities on the trailing hemisphere ($\tilde{\phi} = 0^\circ$) than on the leading hemisphere ($\tilde{\phi} = 180^\circ$) due to sputtering not being uniform over the surface of Europa (Pospieszalska & Johnson, 1989). To take the sublimated and sputtered components of the atmosphere into account, the described neutral density distribution consists of two exponential functions with different surface densities (n_{10}, n_{20}) and scale heights (h_{s1}, h_{s2}) (Jia et al., 2018). The water vapor plume is implemented as an atmospheric inhomogeneity, and its analytic description is based on equation (4) from Jia et al. (2018):

$$N_p = N_{P0} \exp\left(\frac{R_E - r}{H_p} - \left(\frac{\theta}{\theta_p}\right)^2\right). \quad (2)$$

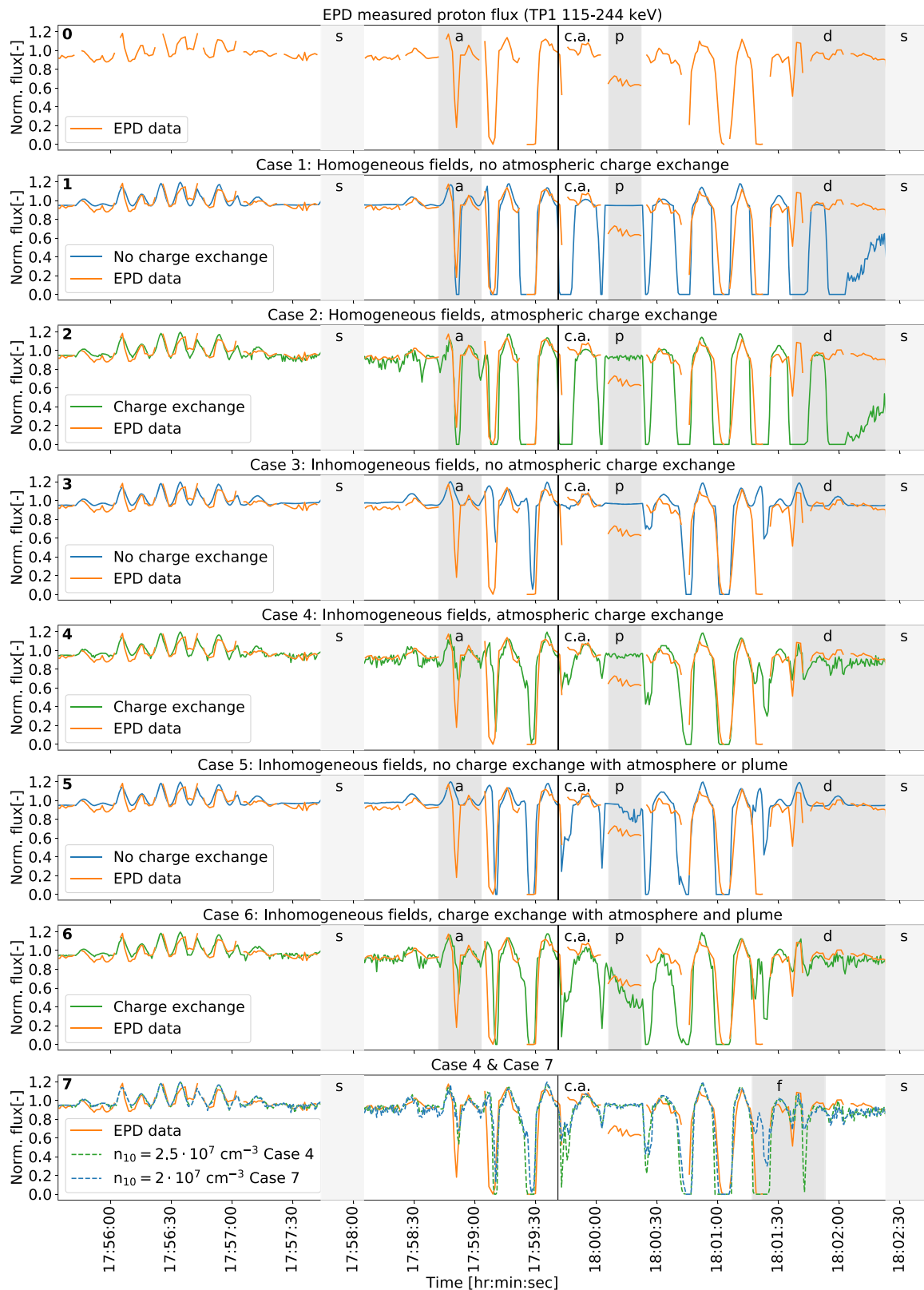


Figure 1. Comparison between the measured proton flux and the simulated flux (both normalized). From top to bottom: EPD proton flux data, followed by Cases 1 to 7. Black solid vertical line: time of the closest approach (c.a.). Light gray boxes marked “s”: times when the instrument moves behind the foreground shield. Marked dark gray boxes (“a,” “p,” “d,” and in the last panel “f”): regions of special interest for the discussion.

Its density distribution has a conical structure and is characterized by the surface density N_{p0} , scale height H_p , and opening angle θ_p . $\tilde{\theta}$ is the polar angle measured relative to the central axis of the plume. The location of the plume was adopted from Arnold et al. (2019).

To determine the contribution of each proton to the flux measured for a specific spacecraft position and instrument pointing, the particle is weighted according to the pitch angle distribution of the flux and the energy distribution of the proton flux away from Europa. Ions are traced until the end of the MHD simulation domain. Since the bounce periods of the protons are around several hundred seconds, they will not encounter Europa again. Based on their pitch angle at the edge of the simulation box, a weighting is applied according to the upstream pitch angle distribution of the proton flux. After binning the particles in 10 logarithmically spaced energy bins, the flux is also weighted according to the energy distribution of the flux, which can be described as a Kappa distribution and which we obtained from Paranicas et al. (2009).

Particles are considered lost and contribute to a decrease in flux, when they impact the surface of Europa or charge exchange with neutrals (from the atmosphere or plume). If the energetic proton charge exchanges, it turns into an energetic neutral atom (ENA), and since it is no longer bound by electromagnetic fields, it escapes the system at a high velocity. The probability of charge exchange with the atmospheric neutrals is determined using equation (3) from Birdsall (1991).

$$P = 1 - \exp(-n_n \sigma g \Delta t) \quad (3)$$

In equation (3), n_n is the density of the neutrals at the location of the particle, σ is the charge exchange cross section, g is the relative velocity, and Δt is the time difference between the integration time steps. Because O₂ is thought to be the major constituent of Europa's atmosphere (Plainaki et al., 2018), we use the charge exchange cross section of H⁺ on O₂ from Basu et al. (1987) for σ . Equation (3) is evaluated at every time step of the particle trajectory. The probability is then compared to a random number from a uniform distribution. If the probability exceeds, the random value charge exchange is assumed to take place. The neutral density is the same as used for the MHD simulations and is described using equations (1) and (2).

3. E26 Flyby Energetic Proton Data

The E26 flyby (3 January 2000) had its closest approach (17:59:43 UT) at an altitude of 348.4 km (Kivelson et al., 2009). The geometry of the flyby can be seen Figure S3. The flux of energetic protons as measured by EPD (115–244 keV, TP1 channel) is shown in the top panel of Figure 1 (orange curve). The flux has been normalized to the mean of the flux during two cycles of the instrument (17:54 to 17:58). This normalization allows for comparison with the particle tracing code, which provides depletions as a percentage. The data has been processed using the software from previous EPD studies, for example, Lagg et al. (2003). The flux is varying due to the scanning motion of the detector, which results in different pitch angles being scanned (see Figure S4). The EPD telescope scans the whole sky in ~120 s using the combined motion of a rotating platform on which it is mounted and the ~20 s period spacecraft spin. Further upstream of Europa, the flux is not affected by Europa (before 17:58). However, near the closest approach (between 17:58 and 18:02), depletions of the energetic proton flux to (nearly) zero occur. These depletions are distinctly different from the flux variation upstream (before 17:58), and we attribute them to the presence of Europa. In this study we focus on the depletions between 17:58 and 18:02. The pitch angle distribution used in the simulation to weight the particles is based on the upstream E26 EPD data. Using the magnetic field vector measured by Galileo's magnetometer, the pitch angle was determined for each measurement. Here a fit of the pitch angle distribution during two instrument cycles (17:54 to 17:58) was made. In Figure 1 it can be seen that the fit (green or blue curve) describes the upstream flux variability well (the complete data from 17:54 is shown in Figure S5).

Every full ~120 s cycle of EPD, the detector moves behind a foreground shield (marked "s" in Figure 1). Behind the radiation shield, the flux level decreases more than 2 orders of magnitude, indicating that the measured signal is not significantly affected by penetrating radiation.

4. Simulations of the Energetic Proton Flux for the E26 Flyby

To investigate the importance of the different factors, we compare the following simulation cases. A plot of the MHD simulations and the atmosphere can be seen in Figure S6.

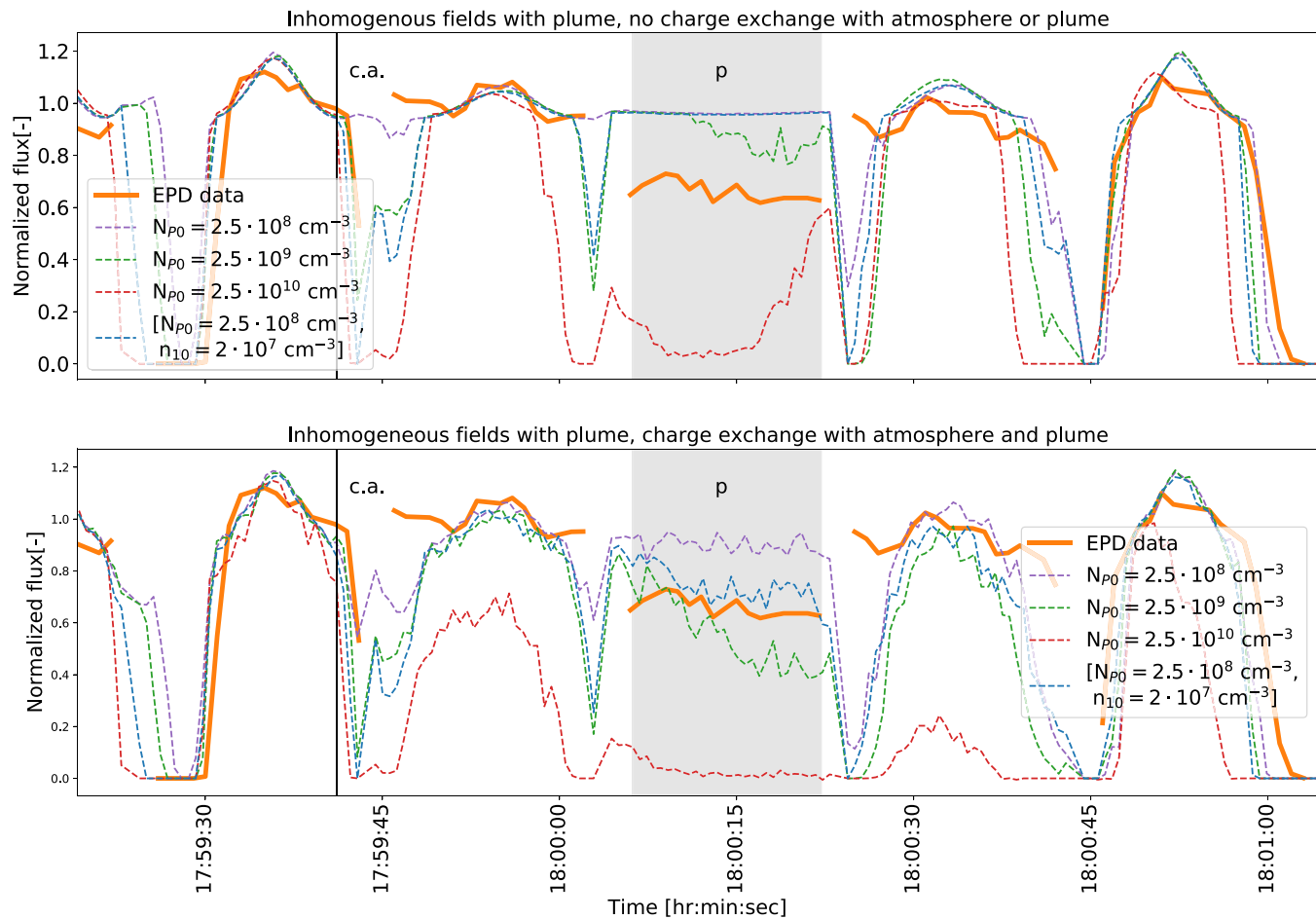


Figure 2. Zoom in on the region between 17:59 and 18:01 from Figure 1 for Cases 5 and 6 (green dashed curve). Also shown are the results of simulations with different (plume) properties. Where the simulation properties differ from the default case (green dashed curve), the differences are mentioned explicitly in the legend.

- Case 1: homogeneous fields, no atmospheric charge exchange.
- Case 2: homogeneous fields, atmospheric charge exchange.
- Case 3: inhomogeneous fields, no atmospheric charge exchange.
- Case 4: inhomogeneous fields, atmospheric charge exchange.
- Case 5: inhomogeneous fields with plume, no charge exchange with the atmosphere or plume.
- Case 6: inhomogeneous fields with plume, charge exchange with the atmosphere and plume.
- Case 7: same as 4 but with a different atmosphere.

Cases 1 and 2, shown in panels 1 and 2 of Figure 1, are generally consistent with the timing of the depletions occurring between 17:58 and 18:02. However, we identify two main inconsistencies between the simulations and the data. First, a depletion feature lasting multiple spins is predicted in the shaded area marked by “d,” which is not present in the data. Second, a depletion occurring shortly after the closest approach in the data, visible in the shaded area marked by “p,” is not reproduced by Case 1 nor Case 2. The addition of charge exchange in Case 2 adds further depletions, at 17:58:30 and at 18:03:00, but has little impact on the feature occurring directly after closest approach visible in the shaded area marked by “p.” This indicates that feature “p” cannot be attributed to charge exchange with the assumed global atmosphere. We consider the simulated depletion marked by “d” and the measured depletion marked by “p” as key differences between the simulation and the data that need to be addressed.

Panels 3 and 4 of Figure 1 show Cases 3 and 4 in which inhomogeneous fields are considered. Compared to Cases 1 and 2, the depletion extending over multiple spins marked by “d” is not predicted in Cases 3 and 4. This indicates that the inhomogeneous fields resulting from the interaction of Europa’s atmosphere

with the magnetospheric plasma plays an important role in the access of energetic protons to the surface and atmosphere. Case 3 differs from Case 1 in the sense that several depletions are no longer predicted (e.g., feature “a”). By introducing atmospheric charge exchange in Case 4, the depletions are reproduced better than in Case 3 (e.g., feature “a”). The only major discrepancy remaining, compared to the data, is the depletion feature in the shaded area marked by “p,” which is not reproduced by the simulation. Case 4 introduces additional minor depletion features, for example, between 18:02:00 and 18:02:30 that do not occur in the data. We attribute the remaining discrepancies between Case 4 and the data to differences between the idealized atmospheric or MHD model and the real atmosphere or magnetospheric environment. In the last panel of Figure 1 we compare Cases 4 to 7, a simulation with a different atmospheric density ($n_{10} = 2 \cdot 10^7 \text{ cm}^{-3}$ instead of $2.5 \cdot 10^7 \text{ cm}^{-3}$). Note that both the MHD and particle tracing simulation have been rerun for this case. Differences between the two cases are visible in the dark gray area marked by “f.” This shows that the simulation is sensitive to changes in atmospheric density less than a factor 2.

In Cases 5 and 6, shown in panels 5 and 6 of Figure 1, inhomogeneous fields are considered, including a plume. Compared to all the previous cases, these are the only cases in which a depletion in the shaded area marked by “p” is reproduced. The depletion in Case 5 is underpredicted compared to the data. Similarly as Case 3, Case 5 is also unable to reproduce some of the major depletion features (e.g., feature “a”), which are reproduced by introducing atmospheric charge exchange in Case 6 (or Case 4). Charge exchange with a plume deepens the depletion in region “p” in Case 6 but also introduces a gradient in the depletion that is not present in the data.

Figure 2 shows a zoom in on the region near the area marked “p” in Figure 1. The fluxes shown by the green dashed lines correspond to Cases 5 and 6 in Figure 1. The results for three additional cases are also shown; the particle tracing and MHD simulation have been rerun for these cases. Two simulations are shown in which the surface density of the plume N_{P0} has been varied to $2.5 \cdot 10^8 \text{ cm}^{-3}$ and $2.5 \cdot 10^{10} \text{ cm}^{-3}$. When N_{P0} is decreased to $2.5 \cdot 10^8 \text{ cm}^{-3}$, there is no distinguishable plume feature. When N_{P0} is increased to $2.5 \cdot 10^{10} \text{ cm}^{-3}$, the simulated depletion is far deeper than measured. A final case is introduced in which the atmospheric surface density n_{10} has been reduced to $2 \cdot 10^7 \text{ cm}^{-3}$. In this case the plume would only cause a depletion when charge exchange with the plume neutrals is taken into account.

5. Discussion

5.1. The Effect of Europa Related Field Perturbations on the Energetic Proton Flux

The comparison of the simulation cases with the data indicates that the simulations with a homogeneous field and a plume-less global atmosphere predict unrealistic depletions that do not occur in the data (Cases 1 and 2, feature “d”). However, by including the inhomogeneous fields resulting from the interaction of Europa’s atmosphere with the magnetospheric plasma, this discrepancy disappears (Cases 3–6). This indicates that the effect of the inhomogeneous fields on the proton trajectories cannot be ignored, as they act to deflect the protons away from the surface and decrease contribution of impacting particles to the total loss observed along the spacecraft trajectory.

5.2. Implications of Charge Exchange on the Energetic Proton Flux

The simulations in Cases 2, 4, 6, and 7 indicate that atmospheric charge exchange with an atmosphere can cause depletions (e.g., feature “a” or “f”), with over 50% of the energetic protons charge exchanging in certain viewing directions of EPD. The atmospheric properties are listed in Table 1 and are within the range suggested by previous studies (Plainaki et al., 2018).

Even though a simulation with inhomogeneous fields does not have the discrepancy addressed in the previous section (Case 3), it does not capture several major depletion features (e.g., feature “a”). The simulation with atmospheric charge exchange (Case 4) does reproduce all the major depletion features, excluding the feature marked “p.” This indicates that charge exchange plays an important role in the depletion of energetic protons and that atmospheric charge exchange at Europa could produce ENAs with over 50% of the energetic protons charge exchanging in certain viewing directions. Charge exchange could therefore also be an important factor that limits access of energetic protons to the surface of Europa, as they can be depleted before they reach the surface.

Some discrepancies (besides feature “p”) between Case 4 and the data remain. We attribute these to differences between the idealized atmospheric or MHD model and the real atmosphere or magnetospheric

environment. Case 7 shows that the fit can be improved by changing the atmospheric properties. We refer a detailed assessment of these differences to a future study.

In the current simulation we have assumed that after charge exchange, the resulting ENA leaves the simulation. However, it is possible that an ENA will re-ionize through multiple collisions in the plume, which could result in depletions being more modest. Since the current simulation is consistent with the data, we assume that these re-ionized energetic particles are not affecting the proton measurement significantly.

5.3. Indications of an Active Plume During E26

A depletion in the shaded area marked by “p” is uniquely reproduced by Cases 5 and 6, which both consider a global atmosphere and plume, thereby indicating the existence of a plume during E26. Even in the case without charge exchange (Case 5), the field perturbations associated with the plume can generate a depletion feature (albeit with an underpredicted magnitude). This indicates that, in the backtracing simulation, the field perturbations associated with a plume can modify the proton trajectories in such a way that they impact on the surface, whereas they would not without a plume. However, Case 6 shows that the depletion is stronger when charge exchange due to the plume is included. This indicates that a plume will be a source of ENAs. Furthermore, by varying the atmospheric density n_{10} (Figure 2), it can be seen that a scenario is possible in which the depletion feature marked by “p” is a consequence of only charge exchange with the plume and not field perturbations. Overall, Case 6 represents the best fit to the data, out of the considered cases. Atmospheric charge exchange with a global atmosphere is required to explain the depletions when the inhomogeneous fields are taken into account.

Due to the large number of free parameters involved and the long computation time of the MHD and particle tracing simulations, we cannot identify a unique best fitting set of parameters. Differences between the data and the simulation remain (e.g., the gradient in the depletion in region “p”); we attribute these to sensitivities of the simulation to the choice of properties of the atmosphere (scale height, surface density, global asymmetries, etc.) and plume (location, density, shape, etc.). For example, compared to the plume used in Arnold et al. (2019), we have not taken into account a tilt of the plume. It is also possible that the plume has a different shape than the conical model applied here. As Berg et al. (2016) has shown, using an advanced DSMC model of the neutrals escaping from a vent on Europa’s surface, a plume could also have a dome like shape, which could have a different effect on the depletion. Furthermore, multiple collisions and stripping/reionization of ENAs within a very dense plume could also be possible but have not been taken into account.

As shown in Figure 2, reducing N_{P0} to $2.5 \cdot 10^8 \text{ cm}^{-3}$ removes the plume feature, while increasing it to $2.5 \cdot 10^{10} \text{ cm}^{-3}$ creates a depletion that is too deep. The range $2.5 \cdot 10^8 \text{ cm}^{-3} < N_{P0} < 2.5 \cdot 10^{10} \text{ cm}^{-3}$ is consistent with previous studies by Jia et al. (2018) and Arnold et al. (2019), which assumed values for N_{P0} of, respectively, $2 \cdot 10^9 \text{ cm}^{-3}$ and $3.9 \cdot 10^9 \text{ cm}^{-3}$. The column densities resulting from these previous studies $7.8 \cdot 10^{20} \text{ m}^{-2}$ for Arnold et al. (2019) and $3 \cdot 10^{20} \text{ m}^{-2}$ for Jia et al. (2018) are within the range determined from HST observations: $1.5 \cdot 10^{20} \text{ m}^{-2}$ for Roth et al. (2014) to $2.3 \cdot 10^{21} \text{ m}^{-2}$ (Sparks et al., 2016), and those from Keck: $0.14 \cdot 10^{20} \text{ m}^{-2}$ (Paganini et al., 2019). The range in column density resulting from this study, $0.5 \cdot 10^{20} \text{ m}^{-2}$ to $5 \cdot 10^{21} \text{ m}^{-2}$, also falls in the range derived from the Keck/HST observations.

6. Conclusion

For flyby E26 we find that the depletions of energetic protons (115–244 keV) are reproduced by a simulation that takes into account the perturbations of the fields as calculated by an MHD simulation and charge exchange with a global atmosphere. Furthermore, a depletion feature occurring shortly after closest approach can be explained by plume associated charge exchange, or a combination with plume associated field perturbations. We therefore conclude, with a new method and an independent data set, that Galileo could have encountered a plume during the E26 flyby as predicted by Blöcker et al. (2016) and Arnold et al. (2019). The inhomogeneous fields resulting from the interaction of Europa’s atmosphere with the magnetospheric plasma and atmospheric charge exchange, including the effect of plumes, play an important role in the motion of energetic protons near Europa and can contribute to their depletion.

Large uncertainties remain in the properties (density profile, 3-D structure, and temporal variability) of Europa’s tenuous atmosphere and plumes (Plainaki et al., 2018). This study emphasizes that energetic ions

are an important tool that can contribute to the detection and characterization of Europa's tenuous atmospheres and plumes and probe its moon-magnetosphere interaction, independently of other methods. This is in particular relevant for the upcoming JUICE mission (Grasset et al., 2013), which has the instrumentation to detect, both energetic ions and ENAs, using the Particle Environment Package (PEP) (Barabash et al., 2016).

Acknowledgments

We acknowledge Kostas Dialynas (charge exchange cross sections), Andrew Poppe (EPD pointing), Andreas Lagg (EPD data software), Peter Kollmann (EPD energy range), the 2019 Europlanet workshop "Outer planet moon-magnetosphere interactions," the ESA/ESTEC Science Faculty for enabling a research visit by A. Blöcker, the Swedish Institute of Space Physics, the Max Planck Institute for Solar System Research, and the International Max Planck Research School for Solar System Science. A. Blöcker received funding from the European Union's Horizon 2020 research and innovation programme under the Marie Skłodowska-Curie Grant Agreement 800586. The MHD simulations were performed on resources provided by the Swedish National Infrastructure for Computing (SNIC) at the PDC Center for High Performance Computing, KTH Royal Institute of Technology. EPD data are available at the NASA Planetary Data System (<https://pds-ppi.igpp.ucla.edu/mission/Galileo/GO/EPD>). The simulations are available online (<http://doi.org/10.5281/zenodo.3752643>).

References

- Arnold, H., Liuzzo, L., & Simon, S. (2019). Magnetic signatures of a plume at Europa during the Galileo E26 flyby. *Geophysical Research Letters*, 46, 1149–1157. <https://doi.org/10.1029/2018GL081544>
- Barabash, S., Brandt, P. C., Wurz, P., & the PEP team (2016). Particle environment package (PEP) for the ESA JUICE mission. American Astronomical Society, DPS meeting # 48.
- Basu, B., Jasperse, J. R., Robinson, R. M., Vondrak, R. R., & Evans, D. S. (1987). Linear transport theory of auroral proton precipitation: A comparison with observations. *Journal of Geophysical Research*, 92(A6), 5920–5932. <https://doi.org/10.1029/JA092iA06p05920>
- Berg, J. J., Goldstein, D. B., Varghese, P. L., & Trafton, L. M. (2016). DSMC simulation of Europa water vapor plumes. *Icarus*, 277, 370–380. <https://doi.org/10.1016/j.icarus.2016.05.030>
- Birdsall, C. K. (1991). Particle-in-cell charged-particle simulations, plus Monte Carlo collisions with neutral atoms, PIC-MCC. *IEEE Transactions on Plasma Science*, 19(2), 65–85. <https://doi.org/10.1109/27.106800>
- Blöcker, A., Saur, J., & Roth, L. (2016). Europa's plasma interaction with an inhomogeneous atmosphere: Development of Alfvén winglets within the Alfvén wings. *Journal of Geophysical Research: Space Physics*, 121, 9794–9828. <https://doi.org/10.1002/2016JA022479>
- Blöcker, A., Saur, J., Roth, L., & Strobel, D. F. (2018). MHD modeling of the plasma interaction with Io's asymmetric atmosphere. *Journal of Geophysical Research: Space Physics*, 123, 9286–9311. <https://doi.org/10.1029/2018JA025747>
- Breer, B. R., Liuzzo, L., Arnold, H., Andersson, P. N., & Simon, S. (2019). Energetic ion dynamics in the perturbed electromagnetic fields near Europa. *Journal of Geophysical Research: Space Physics*, 124, 7592–7613. <https://doi.org/10.1029/2019JA027147>
- Carnielli, G., Galand, M., Leblanc, F., Leclercq, L., Modolo, R., Beth, A., et al. (2019). First 3D test particle model of Ganymede's ionosphere. *Icarus*, 330, 42–59. <https://doi.org/10.1016/j.icarus.2019.04.016>
- Cassidy, T. A., Paranicas, C. P., Shirley, J. H., Dalton III, J. B., Teolis, B. D., Johnson, R. E., et al. (2013). Magnetospheric ion sputtering and water ice grain size at Europa. *Planetary and Space Science*, 77, 64–73. Surfaces, atmospheres and magnetospheres of the outer planets and their satellites and ring systems: Part VIII. <https://doi.org/10.1016/j.pss.2012.07.008>
- Clark, G., Mauk, B. H., Paranicas, C., Kollmann, P., & Smith, H. T. (2016). Charge states of energetic oxygen and sulfur ions in Jupiter's magnetosphere. *Journal of Geophysical Research: Space Physics*, 121, 2264–2273. <https://doi.org/10.1002/2015JA022257>
- Curry, S. M., Liemohn, M., Fang, X., Ma, Y., Slavin, J., Espley, J., et al. (2014). Test particle comparison of heavy atomic and molecular ion distributions at Mars. *Journal of Geophysical Research: Space Physics*, 119, 2328–2344. <https://doi.org/10.1002/2013JA019221>
- De La Fuente Marcos, R., & Nissar, A. (2000). Possible detection of volcanic activity on Europa: Analysis of an optical transient event. *Earth, Moon, and Planets*, 88(3), 167–175. <https://doi.org/10.1023/A:1016561713096>
- Futaana, Y., Barabash, S., Holmstrom, M., Fedorov, A., Nilsson, H., Lundin, R., et al. (2010). Backscattered solar wind protons by Phobos. *Journal of Geophysical Research*, 115, A10213. <https://doi.org/10.1029/2010JA015486>
- Futaana, Y., Machida, S., Saito, Y., Matsuoka, A., & Hayakawa, H. (2003). Moon-related nonthermal ions observed by Nozomi: Species, sources, and generation mechanisms. *Journal of Geophysical Research*, 108(A1), SMP 15–1–SMP 15–10. <https://doi.org/10.1029/2002JA009366>
- Grasset, O., Dougherty, M. K., Coustenis, A., Bunce, E. J., Erd, C., Titov, D., et al. (2013). JUPiter ICY moons Explorer (JUICE): An ESA mission to orbit Ganymede and to characterise the Jupiter system. *Planetary and Space Science*, 78, 1–21. <https://doi.org/10.1016/j.pss.2012.12.002>
- Hayes, J. C., Norman, M. L., Fiedler, R. A., Bordner, J. O., Li, P. S., Clark, S. E., et al. (2006). Simulating radiating and magnetized flows in multiple dimensions with ZEUS-MP. *The Astrophysical Journal Supplement Series*, 165(1), 188–228. <https://doi.org/10.1086/504594>
- Huybrighs, H. L. F., Futaana, Y., Barabash, S., Wieser, M., Wurz, P., Krupp, N., et al. (2017). On the in-situ detectability of Europa's water vapour plumes from a flyby mission. *Icarus*, 289, 270–280. <https://doi.org/10.1016/j.icarus.2016.10.026>
- Jia, X., Kivelson, M. G., Khurana, K. K., & Kurth, W. S. (2018). Evidence of a plume on Europa from Galileo magnetic and plasma wave signatures. *Nature Astronomy*, 2, 459–464. <https://doi.org/10.1038/s41550-018-0450-z>
- Kivelson, M. G., Khurana, K. K., & Volwerk, M. (2009). Europa's interaction with the Jovian magnetosphere. In R. T. Pappalardo, W. B. McKinnon, & K. Khurana (Eds.), *Europa* (pp. 545–570). Tucson: University of Arizona Press.
- Kollmann, P., Paranicas, C., Clark, G., Roussos, E., Lagg, A., & Krupp, N. (2016). The vertical thickness of Jupiter's Europa gas torus from charged particle measurements. *Geophysical Research Letters*, 43, 9425–9433. <https://doi.org/10.1002/2016GL070326>
- Kotova, A., Roussos, E., Krupp, N., & Dandouras, I. (2015). Modeling of the energetic ion observations in the vicinity of Rhea and Dione. *Icarus*, 258, 402–417. <https://doi.org/10.1016/j.icarus.2015.06.031>
- Lagg, A., Krupp, N., & Woch, J. (2003). In-situ observations of a neutral gas torus at Europa. *Geophysical Research Letters*, 30(11), 1556. <https://doi.org/10.1029/2003GL017214>
- Lee-Payne, Z., Kollmann, P., Grande, M., & Knight, T. (2020). Correction of galileo energetic particle detector, composition measurement system high rate data: Semiconductor dead layer correction. *Space Science Reviews*, 216(1), 5. <https://doi.org/10.1007/s11214-019-0621-y>
- Liuzzo, L., Simon, S., & Regoli, L. (2019). Energetic electron dynamics near Callisto. *Planetary and Space Science*, 179, 104726. <https://doi.org/10.1016/j.pss.2019.104726>
- McGrath, M. A., & Sparks, W. B. (2017). Galileo ionosphere profile coincident with repeat plume detection location at Europa. *Research Notes of the AAS*, 1(1), 14.
- Nénon, Q., & André, N. (2019). Evidence of Europa neutral gas torii from energetic sulfur ion measurements. *Geophysical Research Letters*, 46, 3599–3606. <https://doi.org/10.1029/2019GL082200>
- Norman, M. L. (2000). Introducing ZEUS-MP: A 3D, parallel, multiphysics code for astrophysical fluid dynamics. *Astrophysical Plasmas: Codes, Models, and Observations*, 9(66–71).
- Paganini, L., Villanueva, G. L., Roth, L., Mandell, A. M., Hurford, T. A., Retherford, K. D., & Mumma, M. J. (2019). A measurement of water vapour amid a largely quiescent environment on Europa. *Nature Astronomy*, 4, 266–272. <https://doi.org/10.1038/s41550-019-0933-6>
- Paranicas, C., Cooper, J. F., Garrett, H. B., Johnson, R. E., & S.J., S. (2009). Europa's radiation environment and its effects on the surface. In R. T. Pappalardo, W. B. McKinnon, & K. Khurana (Eds.), *Europa* (pp. 529–544). Tucson: University of Arizona Press.

- Paranicas, C., Mauk, B. H., Khurana, K., Jun, I., Garrett, H., Krupp, N., & Roussos, E. (2007). Europa's near-surface radiation environment. *Geophysical Research Letters*, 34, L15103. <https://doi.org/10.1029/2007GL030834>
- Paranicas, C., McEntire, R. W., Cheng, A. F., Lagg, A., & Williams, D. J. (2000). Energetic charged particles near Europa. *Journal of Geophysical Research*, 105(A7), 16,005–16,015. <https://doi.org/10.1029/1999JA000350>
- Plainaki, C., Cassidy, T. A., Shematovich, V. I., Milillo, A., Wurz, P., Vorburger, A., et al. (2018). Towards a global unified model of Europa's tenuous atmosphere. *Space Science Reviews*, 214(1), 40. <https://doi.org/10.1007/s11214-018-0469-6>
- Poppe, A. R., Fatemi, S., & Khurana, K. K. (2018). Thermal and energetic ion dynamics in Ganymede's magnetosphere. *Journal of Geophysical Research: Space Physics*, 123, 4614–4637. <https://doi.org/10.1029/2018JA025312>
- Pospieszalska, M. K., & Johnson, R. E. (1989). Magnetospheric ion bombardment profiles of satellites: Europa and Dione. *Icarus*, 78(1), 1–13.
- Regoli, L. H., Coates, A. J., Thomsen, M. F., Jones, G. H., Roussos, E., Waite, J. H., et al. (2016). Survey of pickup ion signatures in the vicinity of titan using CAPS/IMS. *Journal of Geophysical Research: Space Physics*, 121, 8317–8328. <https://doi.org/10.1002/2016JA022617>
- Roth, L., Saur, J., Retherford, K. D., Strobel, D. F., Feldman, P. D., McGrath, M. A., & Nimmo, F. (2014). Transient water vapor at Europa's south pole. *Science*, 343(6167), 171–174. <https://doi.org/10.1126/science.1247051>
- Selesnick, R. S., & Cohen, C. M. S. (2009). Charge states of energetic ions in Jupiter's radiation belt inferred from absorption microsignatures of Io. *Journal of Geophysical Research*, 114, A01207. <https://doi.org/10.1029/2008JA013722>
- Sparks, W. B., Hand, K. P., McGrath, M. A., Bergeron, E., Cracraft, M., & Deustua, S. E. (2016). Probing for evidence of plumes on Europa with HST/STIS. *The Astrophysical Journal*, 829(2), 121.
- Sparks, W. B., Richter, M., deWitt, C., Montiel, E., Russo, N. D., Grunsfeld, J. M., et al. (2019). A search for water vapor plumes on Europa using SOFIA. *The Astrophysical Journal*, 871(1), L5. <https://doi.org/10.3847/2041-8213/aafb0a>
- Sparks, W. B., Schmidt, B. E., McGrath, M. A., Hand, K. P., Spencer, J. R., Cracraft, M., & Deustua, S. E. (2017). Active cryovolcanism on Europa? *The Astrophysical Journal*, 839(2), L18. <https://doi.org/10.3847/2041-8213/aa67f8>
- Williams, D. J., McEntire, R. W., Jaskulek, S., & Wilken, B. (1992). The galileo energetic particles detector. *Space Science Reviews*, 60(1), 385–412. <https://doi.org/10.1007/BF00216863>
- Wulms, V., Saur, J., Strobel, D. F., Simon, S., & Mitchell, D. G. (2010). Energetic neutral atoms from titan: Particle simulations in draped magnetic and electric fields. *Journal of Geophysical Research*, 115, A06310. <https://doi.org/10.1029/2009JA014893>